JOURNAL OF AIRCRAFT
Vol. 37, No. 2, March–April 2000

Measurements of Bound and Wake Circulation on a Helicopter Rotor

Mahendra J. Bhagwat* and J. Gordon Leishman†
University of Maryland, College Park, Maryland 20742

High-resolution measurements of the three-dimensional velocity field around the blade and in the wake of a small-scale hovering rotor were made using three-component laser Doppler velocimetry. The tip-vortex circulation strength was determined from velocity field measurements in the rotor wake. The spanwise circulation distribution was estimated from the velocity field measurements around each spanwise blade section. It is shown that for helicopter rotors it is difficult to exclude the effects of the returning wake vorticity from contours that enclose the blade section, making unique, grid-independent, bound circulation measurements possible only under very specific conditions. The connection between blade circulation loading and the tip-vortex circulation was also examined. For the configurations studied the initial circulation strength of the tip vortices was found to be approximately 70% of the estimated peak circulation on the blades.

Nomenclature

A	= rotor disk area, πR^2, m^2
C_T	= rotor thrust coefficient, $T/\rho A\Omega^2 R^2$
c	= rotor blade chord, m
$\boldsymbol{ds}$	= directed line segment, m
L	= lift force, N
l_C	= length of integration contour, m
N_b	= number of blades
R	= rotor radius, m
u_T, v_T, w_T	= velocities in traverse coordinates, m s^{-1}
$\boldsymbol{V}$	= velocity vector, m s^{-1}
V_∞	= freestream velocity, m s^{-1}
v_r, v_θ, v_z	= vortex induced radial, swirl, and axial velocities, m s^{-1}
x, y, z	= rotor coordinate system, m
x_T, y_T, z_T	= traverse coordinate system, m
Γ	= circulation, m^2 s^{-1}
Γ_b	= blade bound circulation, m^2 s^{-1}
Γ_v	= tip-vortex circulation strength, m^2 s^{-1}
ζ	= wake age, deg
ρ	= fluid density, kg m^3
σ	= rotor solidity
Ω	= rotor rotational speed, rad s^{-1}

Subscripts

C	= contour of integration
i	= index along integration contour
T	= traverse coordinate system

Introduction

ONE key to improved predictions of helicopter rotor performance, blade airloads, vibrations, and propagated noise lies in an improved understanding and modeling capability of the structure of the rotor tip vortices and their relationship to the basic blade-loading parameters. Tip vortices are lift-generated vortices, i.e., the formation and roll-up process is related to the magnitude and distribution of aerodynamic loading on the generating blade. The wake behind the blade has a circulation strength that is related to the spanwise (radial) derivative of the bound circulation. Typically, the strength of the trailed circulation is highest near the outer edge (tip) and results in the roll up and formation of a strong tip vortex. The actual roll up of vorticity into the tip vortex is a complicated physical process that is not completely understood, but most vorticity in the resulting tip vortex is contained in a small region known as the viscous vortex core. As the vortex convects downstream, the vorticity in the core diffuses through the action of viscosity and turbulence production. As a result, the core size increases with time, and the magnitude of the induced velocities decreases with time. There is only limited experimental data on the tip-vortex formation and viscous diffusion process,[1–3] especially for rotors.[4,5] However, the relatively high vortex strengths and small size of the viscous core results in high induced velocities that produce large time-varying local aerodynamic loads on other blades. These unsteady blade loads are a major contributor to rotor vibrations and are also a source of obtrusive noise.

Over the past two decades several aeromechanical analyses have been developed to model the rotor wake and predict the rotor-wake geometry, the induced inflow through the rotor disk, and the unsteady blade loads (see Refs. 6–11). The success of these methodologies has been limited, in part, because of the strong interdependence of bound circulation and wake circulation. The formation of the tip vortices in terms of strength and location is given by the spanwise (radial) bound circulation distribution. The bound circulation itself depends on the geometry of the vortical wake through the induced velocity at the rotor blades. Therefore, one motivation for the present work was to attempt simultaneous measurements of both the bound and wake circulation for a hovering rotor and to gain an improved insight into the physical mechanism of roll up and subsequent evolution of the tip vortex.

Theoretical description of the tip-vortex roll-up process requires a numerical solution to the Navier–Stokes equations. There are many well-known numerical difficulties and high costs associated with solving this problem. Therefore, simpler models have been used to predict the rolled-up wake of both fixed wings[12–15] and rotating wings.[16] These models have their origins in the work of Betz,[17] where the strength and location of a trailed vortex (or vortices) is related to the distribution of bound circulation along the wing or blade span. References 13–15 give good summaries of the theoretical approaches. Most Betz-type roll-up models have been found to give a reasonable agreement with experimental measurements in the wake of fixed wings.[14,15] However, the nonlinear effects, which are more apparent in case of rotary wings, must be included through semi-empirical parameters to achieve acceptable predictive capabilities.[15,18] Some methods may include submodels of the swirl and axial velocity field close to the vortex core

Received 24 August 1998; revision received 14 June 1999; accepted for publication 30 August 1999.

*Graduate Research Assistant, Department of Aerospace Engineering. Member AIAA.

†Associate Professor, Department of Aerospace Engineering. Senior Member AIAA.

and the subsequent viscous diffusion and dissipation of the tip vortices in the far field. Because of the lack of relevant measurements on rotors,[18–20] the necessary modeling parameters have often been extracted or extrapolated from fixed-wing measurements, e.g., Refs. 21–24.

Whereas high-fidelity experimental measurements of the flow structures as well as the bound circulation on lifting wings are necessary to validate roll-up models, and also to gain an improved insight into the physics of tip-vortex formation, bound circulation measurements can also allow calculation of lift distribution when instrumentation limitations or small scale of the experimental setup may not allow direct measurements of airloads from pressure distributions.[25,26] This can be approached using the well-known Kutta–Joukowski (K–J) theorem. However, to obtain a unique value of integrated circulation that can be related to the sectional lift, the contour of integration must be chosen carefully to ensure that the only source of vorticity contained within it is the bound vorticity on the lifting surface. As discussed by Taylor,[27] contributions to the computed sectional circulation from vorticity in the shed wake can be avoided if appropriate branches of the integration contour are made perpendicular to the shed wake. In the case of fixed wings, this technique can be successfully applied to determine the aerodynamic loading because the wake structure is relatively simple except at the wing tip, e.g., Refs. 24, 28–30. However, for rotary wings the complexity and returning nature of the vortical wake make it unlikely that integration contours which totally isolate the effects of the shed and trailed wake from the blade, can be uniquely chosen.

Circulation measurement techniques have been attempted on helicopter rotors to determine aerodynamic loads, e.g., Refs. 10, 31–35, in part because of the difficulties and expense of instrumenting blades with extensive arrays of pressure sensors. Probe proximity issues to the rotating blades mean that velocity field measurements are only possible using nonintrusive techniques such as laser Doppler velocimetry (LDV). Hoad[31] used a two-component LDV system and showed that for rotors the blade circulation measurements are very sensitive to the shape and size of integration path, but offered no satisfactory guidelines for the choosing the right integration paths. Biggers et al.[32] suggested choosing small integration contours to avoid influence from the tip vortices from a previous blade passage. Although it is necessary that the tip vortex does not enter the integration path, it is not a sufficient condition to ensure proper circulation measurements. The high tip-vortex induced velocities make the flowfield near the blade highly three-dimensional, and in some cases the application of the K–J theorem becomes questionable. Lorber et al.[33] have attempted to confirm the validity of the bound circulation measurements obtained using LDV by comparisons with blade-pressure distributions. Good agreement was suggested in the regions where the flow was assumed to be two-dimensional, and there was no influence from tip vortices from other blades. Berenger et al.[34] showed comparison of numerical predictions of the rotor loading with bound circulation measurements on a two-bladed rotor system. The contour integration paths in these experiments were arbitrarily fixed, and the effects of the returning wake were not carefully examined.

In all previous work on rotor bound circulation measurements, considerable ambiguity remains in the results because values of sectional circulation on the blades were not uniquely determined. Therefore, the objectives of the present work were to examine the velocity integration technique for circulation measurements and to more carefully assess its limitations for rotary-wing applications. The emphasis is placed on obtaining unique, grid-independent values of circulation at each spanwise location. The measurements were conducted using three-component LDV on high spatial and temporal resolution grids. The effect of the trailed wake structure from preceding blades on the radial bound circulation distribution on the following blades was studied. These interactions are important because the proximity to the blade must also have an effect on the evolution of the tip vortices. This is of interest not only during the initial roll up of the tip vortices but also at subsequent blade passages. The connection between the radial distribution of circulation on the blade and the circulation trailed into the vortical wake was also examined.

Table 1 Operating conditions for the two-rotor configurations

Rotor	One-bladed	Two-bladed
Number of blades, N_b	1	2
Rotational speed, Ω	2100 rpm, 35 Hz	2010 rpm, 33.5 Hz
Blade radius, R	406.4 mm	406.4 mm
Blade chord, c	42.5 mm	42.5 mm
Collective pitch, θ_0	4 deg	5 deg
Thrust coefficient, C_T	0.003	0.006
Blade loading, C_T/σ	0.09	0.09

Description of the Experiment

Rotor System

The experimental setup consisted of teetering-type rotors driven by a three-phase constant torque electrical motor. An integral shaft encoder provided a once-per-revolution signal for phase-locked synchronization. Both one- and two-bladed rotors were used for the experiments. The single-bladed rotor used a counterweight for balance, whereas the two-bladed rotor used a set of aerodynamically and dynamically matched blades. All blades were dynamically stiff. The rotor blades had a rectangular planform with a radius of 406.4 mm and a chord of 42.5 mm, with a root cutout of 20% of rotor radius. The airfoil shape was a NACA 2415. Untwisted blades were used to keep the thrust distribution biased toward the blade tip so that a relatively strong tip vortex was generated. The operating conditions for the rotors were chosen to give the same nominal blade loading C_T/σ and, therefore, the same nominal initial tip-vortex strength. For both rotors the tip Mach number was approximately 0.26, with a corresponding tip chord Reynolds number of 2.7×10^5. Table 1 summarizes the operating conditions for the two rotors.

LDV System

A fiber-optic-based three-component LDV system was used to make measurements of the velocity field. A 6-W multiline argon-ion laser-produced laser light in the 457.9–528.7-nm band. A beam separator consisting of a dispersion prism split the single multiline laser beam into three colors. The beam separator produced a matrix of six beams; two green beams at 514.5 nm, two blue beams at 488 nm, and two violet beams at 476.5 nm. One beam of each color was shifted in frequency by 10 MHz using a Bragg cell.

The beams were then focused by couplers into single-mode polarization-preserving fiber optic lines, which carried the laser light to the transmitting optics. The transmitting and receiving optics were contained in a pair of fiber optic probes (see Fig. 1). One probe was used for the green and blue beams and the other for the violet beams. The beams were collimated when they emerged from the fiber optic lines, passed through a transmitting lens, and focused to a point to form the measurement volume. Beam expanders connected to each probe enhanced the spatial resolution and improved the signal-to-noise ratio.

Both the fiber-optic probes and, therefore, the LDV measurement volume were moved by a three-axis traverse (see Fig. 1) and remotely controlled by the data acquisition software. Different coordinate systems were used during the measurements. The rotor coordinate system had its origin at the rotor hub. This conventional coordinate system was convenient for documenting the rotor-induced velocity fields and the position of the tip-vortex relative to the rotor. The traverse coordinate system was used only for reference and alignment purposes.

The flowfield was seeded with atomized olive oil, which from a calibration was known to produce an average particle size of 0.6 μm with a standard deviation of 0.2 μm. The scattered light from seed particles crossing the interference fringes was collected by the receiving optics and coupled to a set of photomultiplier tubes. The photomultiplier tubes separated the light by color and converted it into analog signals.

A three-channel digital processor was used to process the incoming Doppler signals. Each Doppler signal, which is proportional to the particle velocity, was filtered to remove the pedestal and wideband noise. The resulting signals were then amplified and

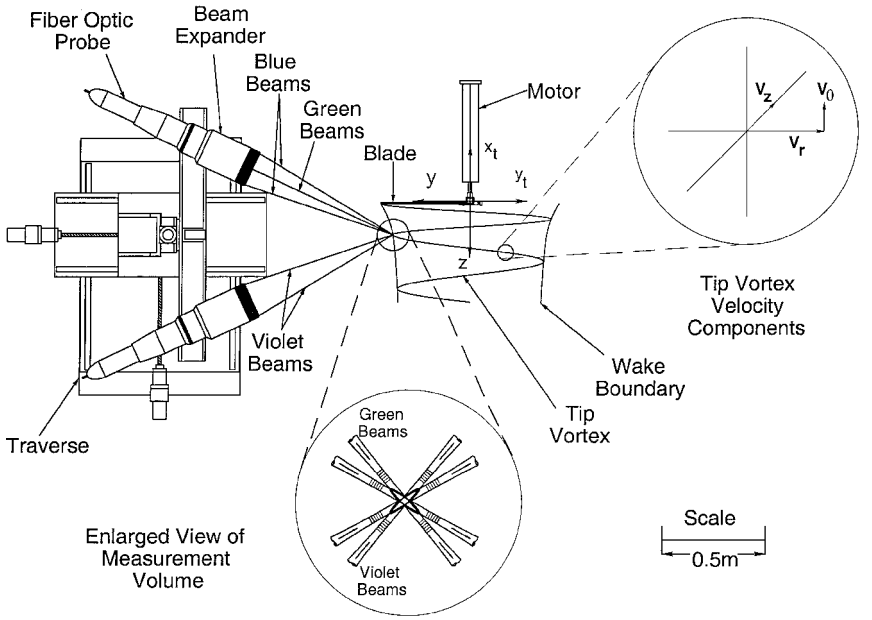

Fig. 1 Schematic of LDV system and rotor showing traverse and vortex coordinate systems.

digitized. A real-time autocorrelator computed the Doppler frequency for each channel, which were then transformed into three velocity components. These three velocity components were then converted into an orthogonal axis system based on the beam crossing angles. The rotary machine resolver interface used the one-per-revolution signal from the shaft encoder to assess continuously the rotor phasing and also sent a 3600 per-revolution signal (phase precision ±0.1 deg) to the LDV processor. This was used to calculate the blade azimuthal location, which was digitally tagged to the velocity data. The azimuth-tagged data were then sorted into 400 discrete bins giving an azimuthal resolution of 0.9 deg. Only data within a short acceptance window were considered valid so that data falling into these bins were always biased toward the leading edge of the bin pulse. A phase-locked loop processor ensured that the data were free from errors introduced by any variations in the rotational speed of the rotor.

LDV is a statistical measurement technique, and, therefore, it is necessary to collect a large number of data samples to obtain statistically meaningful results. In the present measurements all three channels were required to collect 10,000 data samples. All measurements were made in coincidence mode to ensure correlated velocity components on the same particle and with the same statistical accuracy on all channels. Because of the coincidence criteria, the effective LDV measurement volume was approximately spherical with a diameter of 70 μm as defined by three pairs of intersecting ellipsoids (one from each of the green, blue, and violet pairs). The measurement volume contained three sets of approximately 24 interference fringes. The small measurement volume allowed high spatial resolution even in regions of high velocity gradients, like the vortex core.

Seeding can introduce errors in the measured velocity because the seed particle may not travel at the local flow velocity because of acceleration effects. This problem was analyzed in detail in Ref. 36, and for the present choice of olive oil seed particles, with a diameter <1 μm, the errors in the measured velocity are found to be negligible.[37] Aperiodicity of the rotor wake can be a source of uncertainty in the tip-vortex velocity measurements; however, it is possible to correct for this uncertainty using inverse convolution techniques (see Refs. 38 and 39). The aperiodicity of rotor wake was found to be significant only at vortex ages greater than two rotor revolutions; therefore, its influence on the velocity field measurement near the blade section is small, and no corrections have been applied to the data presented in this article.

Test Procedure

Circulation calculations from the measurements around the blade section were made at several spanwise stations. Because of the periodic nature of the flow about the blade of a hovering rotor, the velocity field could be measured along a one-dimensional axial grid, perpendicular to the plane of rotation, as shown in Fig. 2. The time-dependent measurements along this one-dimensional grid were then phase-resolved and mapped to points on a curvilinear spatial grid enveloping the blade section. This allowed reconstruction of the instantaneous velocity field around the blade section. An example of this is shown in Fig. 3, which shows the spanwise (radial) velocity around a blade section of the one-bladed rotor located at 85% rotor radius. There is a strong radial velocity around the blade section, which shows that the flowfield is highly three dimensional. There is also some three dimensionality induced by the trailed wake vortices. Estimates of the bound circulation Γ_b were obtained by numerically evaluating the closed-loop integral of the measured velocity field around a closed counterclockwise contour C, encompassing the blade section, i.e.,

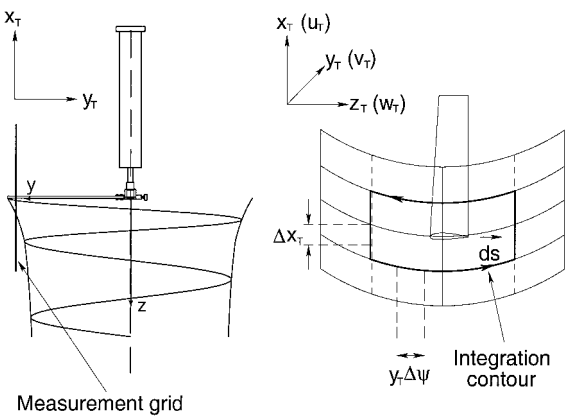

Fig. 2 Schematic of circulation contour in terms of the spatial and temporal grid.

$$\Gamma_b = -\oint_C \boldsymbol{V}\cdot\boldsymbol{ds} = -\sum_{\text{all sides}} u_{T_i}(\Delta x_{T_i}) + w_{T_i}(y_T\Delta\psi)_i \qquad (1)$$

The large grid used in the present measurements allowed for multiple integration paths to examine the sensitivity of Γ_b to the path shape, length, and aspect ratio. Figure 4 shows typical rectangular and square integration paths enclosing the blade section. The effects of curvature of the integration contour are small and can be neglected for all spanwise locations away from the blade root. The blade lift loading can then be determined through application of the

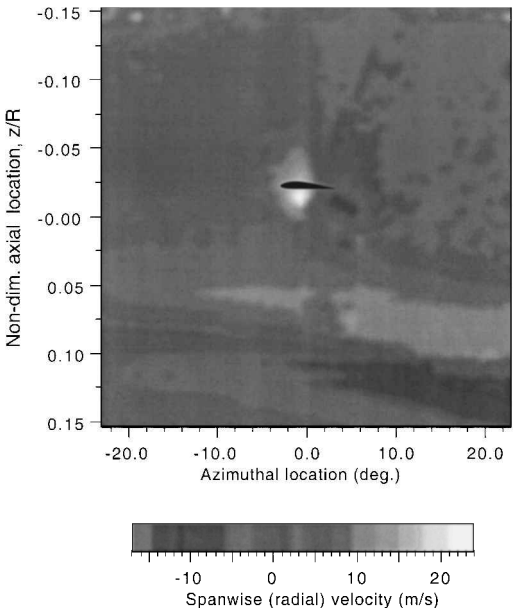

Fig. 3 Instantaneous spanwise (radial) velocity field around a blade section at 85% rotor radius for the one-bladed rotor.

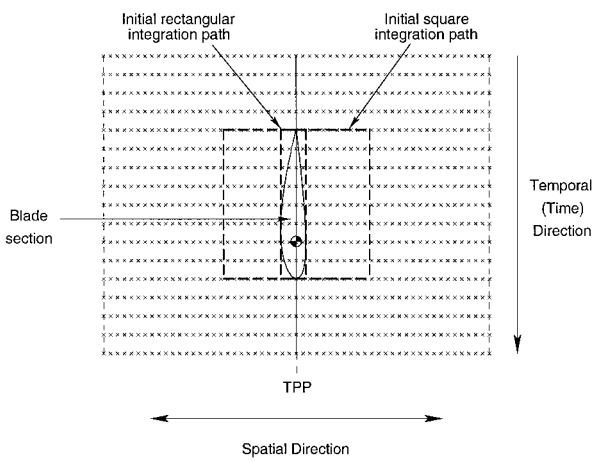

Fig. 4 Schematic showing the rectangular and square integration contours relative to measurement grid.

K–J theorem, which relates the lift on a lifting body L to the bound circulation Γ_b using

$$L = \rho V_\infty \Gamma_b = \rho V_\infty \left(-\oint_C \boldsymbol{V} \cdot \boldsymbol{ds} \right) \tag{2}$$

Results and Discussion

Figure 5 shows typical results of the variation of the bound circulation with increasing length (perimeter) of a rectangular integration contour at three spanwise stations for the one-bladed rotor. The smallest contour that just enclosed the blade section was rectangular, and the integration contour size was increased in all four directions by small increments. For the present results the circulation values initially increased rapidly with increasing grid size, but quickly reached nominally constant values and thereafter remained independent of grid size. These results suggest that, at least for the one-bladed rotor at these operating conditions, there are no significant extraneous contributions to the velocity field from vorticity contained in the rotor wake. Therefore, as previously suggested by Lorber et al.,[33] the results can be considered representative of the blade lift through the application of the K–J theorem.

This is further confirmed by Figs. 6 and 7, which show contours of the vorticity over a plane normal to the blade at two radial stations

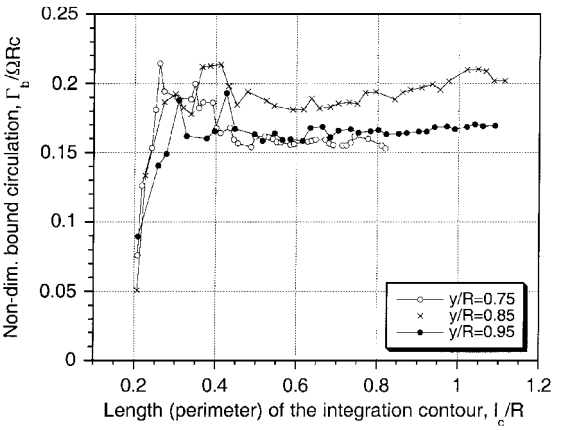

Fig. 5 Bound circulation estimated from measured velocity field at three representative radial blade stations as a function of contour size, $N_b = 1$.

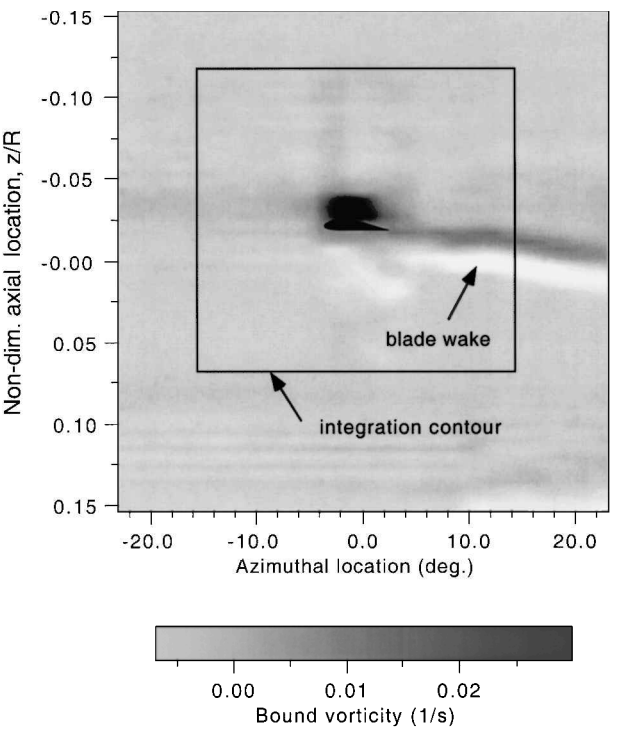

Fig. 6 Contours of vorticity surrounding the blade element, $y/R = 0.85$, $N_b = 1$.

$y/R = 0.85$ and 0.95, respectively. Because of the high spatial resolution of the present measurements, the vorticity could be calculated by numerical differentiation of the measured velocity field in that plane. In both cases it will be seen that nearly all of the vorticity is concentrated near the blade section. Therefore, the circulation technique can be applied simply by ensuring that the contour of integration is large enough to contain all of this vorticity. As shown in Fig. 5, the circulation becomes independent of the integration path as long as it contains all of this vorticity. The wake shed behind the blade contains both positive and negative vorticity; however, because the contour of integration is made nearly perpendicular to the shed wake, the contribution to the computed bound circulation is effectively removed.

Figure 8 shows the corresponding circulation results for the two-bladed rotor as computed over rectangular measurement contour. In this case the circulation evaluated at successive radial stations showed significantly different trends compared to the one-bladed results. At $y/R = 0.95$, however, the behavior was found to be similar

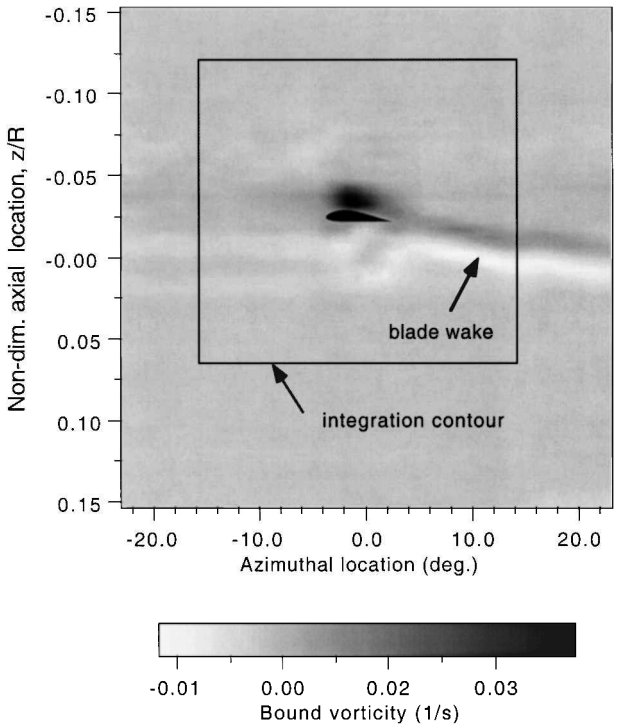

Fig. 7 Contours of vorticity surrounding the blade element, $y/R = 0.95$, $N_b = 1$.

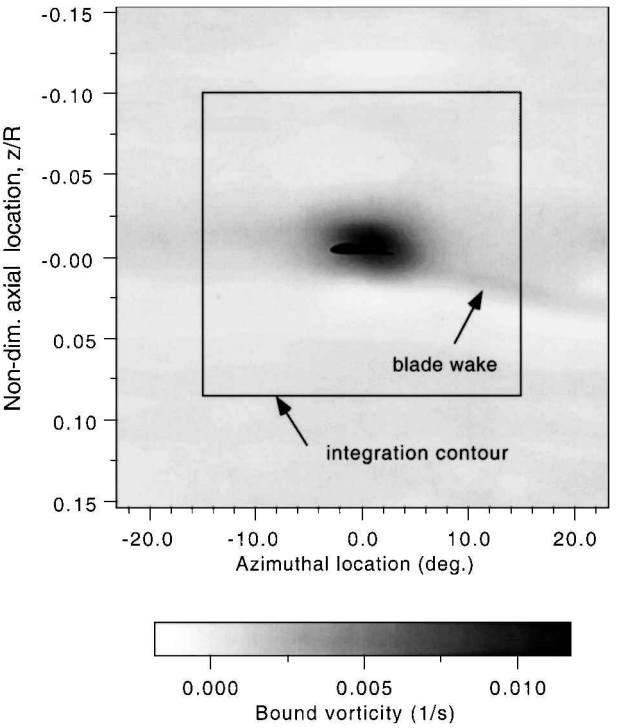

Fig. 9 Contours of vorticity surrounding the blade element, $y/R = 0.95$, $N_b = 2$.

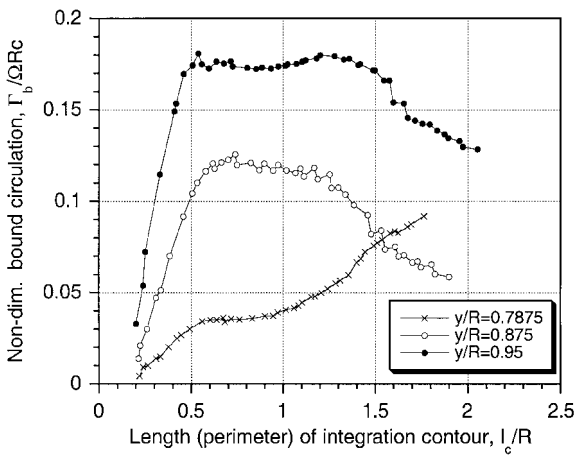

Fig. 8 Bound circulation estimated from measured velocity field at three representative radial blade stations as a function of contour size, $N_b = 2$.

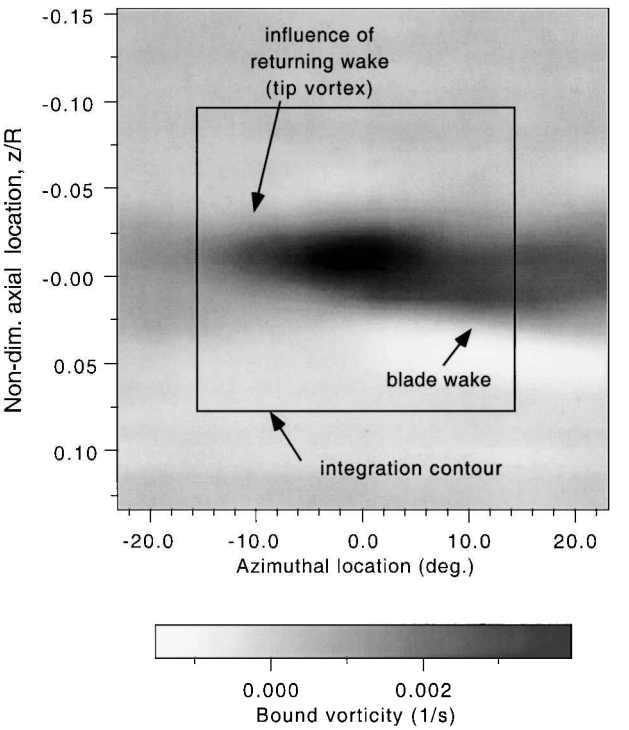

Fig. 10 Contours of vorticity surrounding the blade element, $y/R = 0.88$, $N_b = 2$.

to that for the one-bladed rotor. Here, the circulation increased with the integration path size, reached a maximum value, remained nominally constant for a significant range of grid sizes, and then decreased slowly. This decrease in circulation for larger grid sizes indicates presence of some extraneous vorticity contained in the flowfield. At $y/R = 0.88$ the circulation reached a maximum value and quickly started to decrease. At a further inboard station at $y/R = 0.79$, the circulation continued to increase slowly as the size of the integration contour was increased. These latter results are symptomatic of the presence of extraneous vorticity from the rotor wake being included inside the integration contour.

Figures 9 and 10 show the contours of vorticity at two radial stations for the two-bladed rotor. One station is near the tip ($y/R = 0.95$), and the other is near the radial location of the tip vortex generated by the previous blade ($y/R = 0.88$). In the first example (Fig. 9) the vorticity distribution in the measurement plane was found to be essentially the same as for the one-bladed rotor. The second example in Fig. 10 shows that the vorticity field is significantly affected by the proximity of the tip vortex from a preceding blade. The vorticity in the wake is of a magnitude comparable to the bound vorticity at the blade element and, therefore, has a significant effect on the velocity field in the measurement grid. In this case the computed bound circulation must contain some contributions from the tip vortex below the blade. It is clearly impossible to choose an integration contour that excludes effects of the wake vorticity or a leg that provides a self-cancelling effect. Therefore, as shown in Fig. 8, when the size of the integration contour is increased larger

amounts of wake vorticity are included in the integration, and the circulation decreases.

These examples shown here emphasize the general difficulties in making bound circulation measurements on rotors because of the difficulties in excluding the contributions of returning wake and trailed vortex filaments from the integration path. This is particularly the case for rotors with three or more blades, where the shed wake and tip vortices from preceding blades will generally lie very close to the following blades. As already explained, the integration technique for calculating the circulation is based on the assumption implied by the K–J theorem, that is, only the circulation present inside the closed integration contour is the bound vorticity associated with the blade itself. The presence of a vortical shear layer and/or the tip vortex (or any part thereof) inside the integration contour will result in values of circulation that will not be representative of the blade lift.

The results in Ref. 31 indicate some preference for a rectangular integration path because it may help in limiting the contributions from the wake and/or the tip-vortex filaments, thereby giving a grid-independent, unique value of circulation. To examine the effects of the shape of the integration path, the bound circulation was integrated over a square contour, and the change of circulation with increasing contour size was compared with the results for the rectangular case. Figure 11 shows an example of these results for increasing integration contour size for the two-bladed rotor at a spanwise location of $y/R = 0.95$. Because the square contour was big enough to contain all of the bound vorticity around the blade section, the results did not show a buildup of circulation for small contour sizes. For larger contour sizes the calculated circulation is same for both square and the rectangular integration paths. This confirms that the bound circulation is independent of the shape of the integration contour, as long as the assumption that there is no other vorticity in the closed contour is valid.

Values of average asymptotic circulation at successive radial blade stations have been determined from the results, such as those shown in Figs. 5 and 8. The values of circulation, which were found to remain constant at least over a range of contour sizes, included all of the bound vorticity and did not include any extraneous vorticity contributions. These results for the radial distribution of bound circulation are shown in Figs. 12 and 13. The tip-vortex locations below the tip path plane are also shown to compare the effects of their proximity to the blade. It was not possible to measure the three-dimensional velocity field further inboard than 75% rotor radius because the blade blocked the optical access for one or more laser beams.

The circulation measurements on the one-bladed rotor showed a smooth curve (see Fig. 12a) with the maximum circulation occurring at approximately $y/R = 0.85$. The circulation showed a sharp fall off from the maximum to a small value at the blade tip. Because

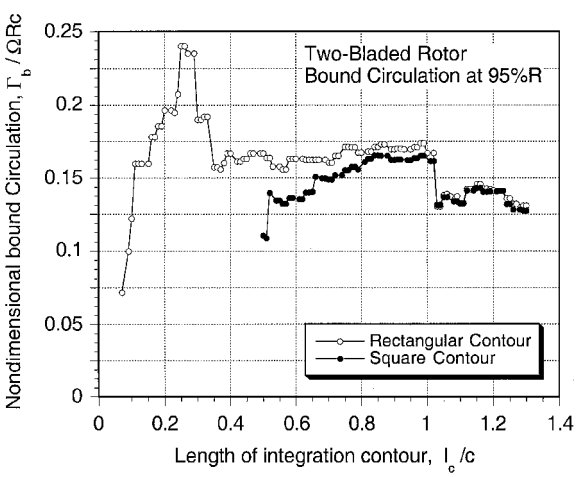

Fig. 11 Bound circulation estimated from measured velocity field for rectangular and square integration contours, $N_b = 2$, $y/R = 0.95$.

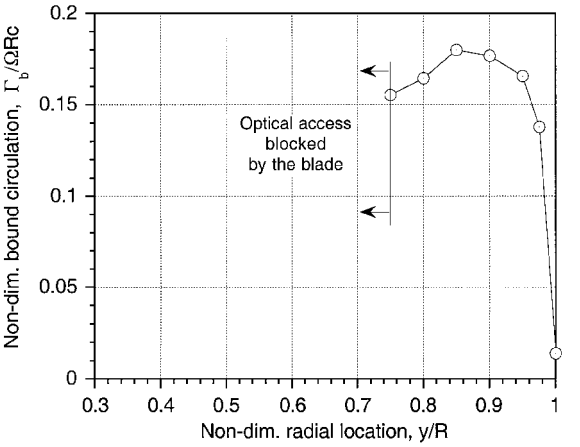

Fig. 12a Measurements of bound circulation along the blade span.

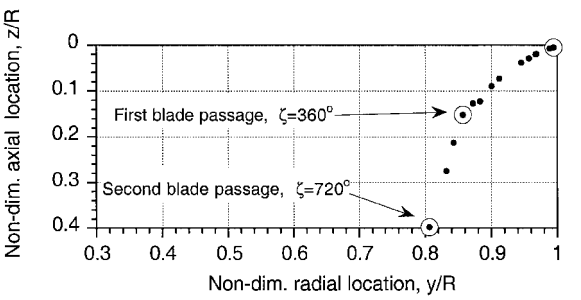

Fig. 12b Corresponding tip-vortex locations, $N_b = 1$.

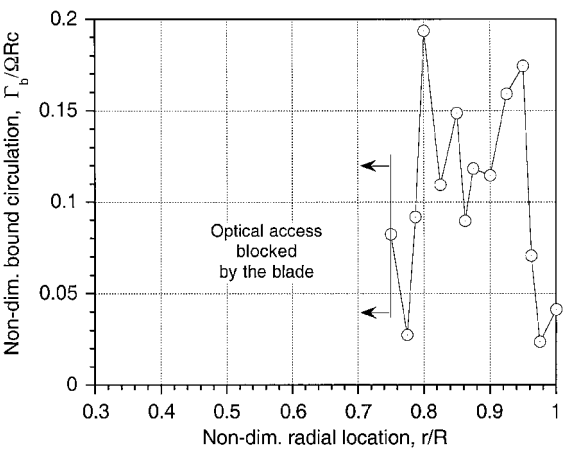

Fig. 13a Measurements of bound circulation along the blade span.

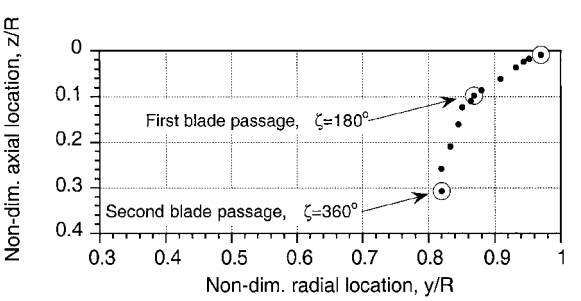

Fig. 13b Corresponding tip-vortex locations, $N_b = 2$.

of the existence of a trailed vortex originating at the blade tip, the velocity field measurements made at the extreme tip must always contain some contributions from the tip vortex to the sectional bound circulation. Figure 12b shows the trajectory of the tip vortex in a radial plane as determined from the LDV measurements, with the locations of the trailed tip vortex at successive blade passages being identified. At the first blade passage the tip vortex lies at approximately $(y/R, z/R) = (0.85, 0.15)$, and therefore it is well outside the contour of integration used to determine the values of bound circulation. These circulation measurements on the one-bladed rotor are, therefore, considered representative of the lift distribution on the blade.

Figure 13a shows the radial distribution of circulation for the two-bladed rotor. These values were determined by selecting values of local circulation that remained nominally constant and independent of grid size. Figure 13a shows large excursions in the circulation distribution compared to the relatively smooth distribution found for the one-bladed rotor. Several additional measurements were made at intermediate stations to confirm the more complicated nature of the bound circulation distribution. Two distinct peaks in the spanwise circulation were seen to occur at approximately $y/R = 0.95$ and 0.80. The measured locations of the tip vortices relative to the blade at the first and the second blade passage are shown in Fig. 13b. The minimum in the circulation distribution at $y/R \approx 0.85$ is clearly correlated with the position of the tip vortex below the blade at the first blade passage. For the two-bladed rotor the tip vortex is located at approximately $(y/R, z/R) = (0.86, 0.1)$ at the first blade passage, and so is considerably closer to the blade than for the one-bladed rotor (Fig. 12). The inverse distance relationship of the induced velocity field from the vortex implies an interaction with the blade that is at least twice as strong. The proximity of the tip vortices to the blade makes the flowfield near the blade highly three dimensional, and so violates the two-dimensionality implied by the K–J theorem. It is, therefore, clear that in some cases the contributions from the tip vortex (in whole or in part) are being included in the contour of integration used to determine the bound circulation. Therefore, as mentioned earlier, this spanwise circulation distribution may not be representative of the blade lift distribution.

The spanwise distribution of the bound circulation results in a trailed vortex sheet behind the blade and roll up of a tip vortex. In rotary-wing flows the tip vortex is well formed with a distinctive finite core at its origin near the trailing of the wing tip. The physics of the roll up of a tip vortex and its relation to the blade loading is hard to predict, e.g., Ref. 15. Using the simple Betz model, the strength of the rolled-up tip vortices should be equal to the magnitude of the peak value of bound circulation on the blade. Figures 12 and 13 show that the peak bound circulation has a nondimensional value of 0.179 for the one-bladed rotor, whereas the two-bladed rotor shows two peaks. The first peak has a value of 0.173 at $y/R = 0.95$, and the second peak has a value of 0.192 at $y/R = 0.8$.

In the rotor wake, velocity field measurements were performed in the tip-vortex cores to establish the structure and the strength of the tip vortices or the trailed circulation. The procedure and detailed results for tip-vortex measurements have been reported in Refs. 4, 37, 40, and 41. Figure 14 shows the tip-vortex circulation as a fraction of the peak bound circulation with increasing wake age. For the two-bladed rotor the maximum value of the measured bound circulation was used. The ordinate in this case is vortex age ζ times the number of blades N_b. This equivalent vortex age ζN_b allows a comparison of the results on a timescale that gives coincident blade passage events. The present results show that the tip-vortex strength near the vortex origin is about 70% of the peak bound circulation. That is, the actual tip-vortex strength is lower than that predicted on the basis of Betz theory, and not all of the vorticity outboard of the peak bound circulation rolls up into the tip vortex. In the present case approximately 70% of the vorticity between the tip and the first peak in bound circulation is contained in the tip vortex. The remaining vorticity is spread over the trailing vortex sheet behind the blade. Thereafter, the circulation contained in the tip vortex dissipates to about 50% of the peak bound circulation.

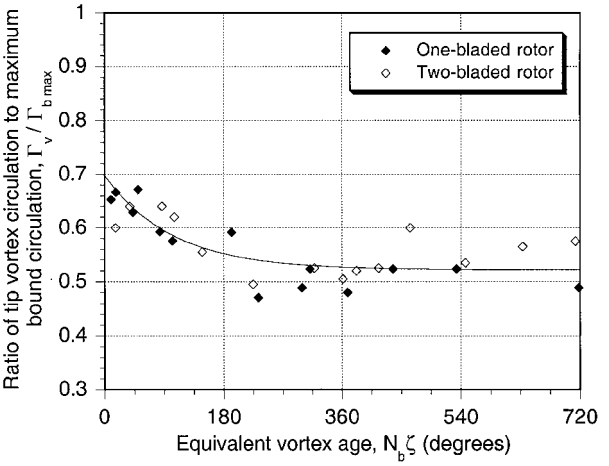

Fig. 14 Circulation strength of the tip vortices as a function of increasing wake age.

Conclusions

The closed-loop contour integration method used for estimating blade-bound circulation on rotor blades is shown to be sensitive to the choice of the integration path. In general, the bound circulation around a blade section is not independent of the integration contour because of the presence of the tip vortex and other wake vorticity near the blade. Conformation to the independence of integration contour is the only way to ensure that the measured bound circulation can be related to the actual aerodynamic lift on the blade. If there is no extraneous vorticity present near the blade section, the measured bound circulation is found to be independent of the shape and size of the integration contour. However, the proximity of tip vortex to the blade causes a substantial underprediction of the sectional bound circulation. Therefore, the technique of velocity field integration to compute bound circulation must be applied with great care, always ensuring that the measured values are grid independent, at least over some range of integration grids. The strength of the tip vortex showed a slowly dissipative trend. For the present configurations the initial strength at the origin of the tip vortex was found be only about 70% of the peak in radial circulation distribution.

Acknowledgments

This work was supported by the National Rotorcraft Technology Center under Grant NCC 2944.

References

[1] Squire, H. B., "The Growth of a Vortex in Turbulent Flow," *Aeronautical Quarterly*, Vol. 16, Aug. 1965, pp. 592, 593.

[2] Mason, W. H., and Marchman, J. F., "Far Field Structure of Aircraft Wake Turbulence," *Journal of Aircraft*, Vol. 10, No. 2, 1973, pp. 87–92.

[3] Iversen, J. D., "Correlation of Turbulent Trailing Vortex Decay Data," *Journal of Aircraft*, Vol. 13, No. 5, 1996, pp. 338–342.

[4] Bhagwat, M. J., and Leishman, J. G., "On the Relationship Between the Blade Lift and the Tip Vortex Characteristics," *Proceedings of the 54th Annual American Helicopter Society Forum*, Washington, DC, 1998.

[5] Mahalingam, R., and Komerath, N. M., "Measurements of the Near Wake of a Rotor in Forward Flight," *Proceedings of the 36th Aerospace Sciences Meeting and Exhibit*, AIAA Paper 98-0692, Reno, NV, 1998.

[6] Clark, D. R., and Leiper, A. C., "The Free Wake Analysis—A Method for Prediction of Helicopter Rotor Hovering Performance," *Journal of the American Helicopter Society*, Vol. 15, No. 1, 1970, pp. 3–11.

[7] Bliss, D. B., Dadone, L., and Wachspress, D. A., "Rotor Wake Modelling for High Speed Applications," *Proceedings of the 43th Annual American Helicopter Society Forum*, 1987.

[8] Johnson, W. R., "Wake Model for Helicopter Rotors in High Speed Flight," NASA CR-1177507, U.S. Army Aviation Systems Command TR-88-A-008, Nov. 1988.

[9] Egolf, T. A., "Rotor Wake Modelling for High Speed Applications," *Proceedings of the 44th Annual American Helicopter Society Forum*, 1988.

[10] Del Bianco, P., Berton, E., Favier, D., and Maresca, C., "Hover Performance Prediction Using a Full Potential Method: Comparison with

Experiments, *Proceedings of AIAA 15th Applied Aerodynamics Conference*, Paper 97-2323, Atlanta, GA, 1997.

[11]Bagai, A., and Leishman, J. G., "Accelerated, High Resolution Free-Vortex Wakes for Rotor Aeroacoustic Analysis," *Proceedings of AIAA 15th Applied Aerodynamics Conference*, Paper 97-2327, Atlanta, GA, 1997.

[12]Rossow, V. J., "On the Inviscid Rolled-Up Structure of Lift Generated Vortices," *Journal of Aircraft*, Vol. 10, No. 11, 1973, pp. 647–650.

[13]Donaldson, C. D., "A Brief Review of the Aircraft Trailing Vortex Problem," Air Force Office of Scientific Research, AFOSR-TR-71-1910, Arlington, VA, July 1971.

[14]Bilanin, A. J., and Donaldson, C. D., "Estimation of Velocities and Roll-Up in Aircraft Wake Vortices," *Journal of Aircraft*, Vol. 12, No. 7, 1975, pp. 578–585.

[15]Rule, J. A., and Bliss, D. B., "Prediction of Viscous Trailing Vortex Structure from Basic Loading Parameters," *AIAA Journal*, Vol. 36. No. 2, 1998, pp. 208–218.

[16]Bliss, D. B., "Prediction of Tip Vortex Self-Induced Parameters in Terms of Rotor Blade Loading," *Proceedings of the American Helicopter Society Technical Specialists' Meeting on Aerodynamics and Aeroacoustics*, Arlington, TX, 1987.

[17]Betz, A., "Behaviour of Vortex Systems," NACA TM 713, 1935.

[18]Johnson, W., "Rotorcraft Aerodynamics Models for a Comprehensive Analysis," *Proceedings of the 54th Annual American Helicopter Society Forum*, 1998.

[19]Johnson, W., "Airloads, Wakes and Aeroelasticity," AGARD-R-781, Nov. 1990.

[20]Leishman, J. G., and Bagai, A., "Challenges in Understanding the Vortex Dynamics of Helicopter Rotor Wakes," *AIAA Journal*, Vol. 36, No. 7, 1998, pp. 1130–1140.

[21]Dosanjh, D. S., Gasparek, E. P., and Eskinazi, S., "Decay of a Viscous Trailing Vortex," *The Aeronautical Quarterly*, Vol. 3, No. 3, 1962, pp. 167–188.

[22]Orloff, K. L., "Trailing Vortex Wind Tunnel Diagnostics with a Laser Velocimeter," *Journal of Aircraft*, Vol. 11, No. 8, 1974, pp. 477–482.

[23]Singh, P. I., and Uberoi, M. S., "Experiments on Vortex Stability of Aircraft Wake Turbulence," *Physics of Fluids*, Vol. 19, No. 12, 1976, pp. 1858–1863.

[24]McAllister, K. W., and Takahashi, R. K., "NACA 0015 Wing Pressure and Trailing Vortex Measurements," NASA TP 3151, Nov. 1991.

[25]Bryant, L. W., and Williams, D. H., "An Investigation of the Flow of Air Around an Aerofoil of Infinite Span," *Philosophical Transactions of the Royal Society, Series A*, Vol. 225, 1925, pp. 199–237.

[26]Fage, A., and Simmons, L. F., "An Investigation of the Air-Flow Pattern in the Wake an Aerofoil of Finite Span," *Philosophical Transactions of the Royal Society, Series A*, Vol. 225, 1925, pp. 303–330.

[27]Taylor, G. I., "Note on the Connection Between the Lift on an Aerofoil in a Wind Tunnel and the Circulation Round It," *Philosophical Transactions of the Royal Society, Series A*, Vol. 225, 1925, pp. 238–245.

[28]Orloff, K. L., "The Spanwise Lift Distribution on a Wing from Flowfield Velocity Survey," *Proceedings of the AIAA 11th Fluid and Plasma Conference*, Seattle, WA, July 1978.

[29]Felker, F. F., Piziali, R. A., and Gall, J. K., "Spanwise Loading Distribution and Wake Velocity Surveys of a Semi-Span Wing," NASA TM 84213 USAARADCOM TR 82-A-1, Feb. 1982.

[30]Desabrais, K. J., and Johari, H., "Direct Circulation Measurement of a Wing Tip Vortex Using Ultrasound," *Proceedings of 36th Aerospace Sciences Meeting and Exhibit*, AIAA Paper 98-0609, Reno, NV, 1998.

[31]Hoad, D. R., "Helicopter Local Blade Circulation Calculations for a Model Helicopter Rotor in Forward Flight Using Laser Doppler Velocimeter Measurements," *Proceedings of the 47th Annual American Helicopter Society Forum*, 1991.

[32]Biggers, J. C., Chu, S., and Orloff, K. L., "Laser Velocimeter Measurements of Rotor Blade Loads and Tip Vortex Rollup," *Proceedings of the 31st Annual American Helicopter Society Forum*, 1975.

[33]Lorber, P. F., Stauter, R. C., and Landgrebe, A., "A Comprehensive Hover Test of the Airloads and Airflow of an Extensively Instrumented Model Helicopter Rotor," *Proceedings of the 45th Annual American Helicopter Society Forum*, 1989.

[34]Berenger, T., Favier, D., Maresca, C., and Berton, E., "Experimental and Numerical Investigation of Rotor Aerodynamics in Forward Flight," *Proceedings of 34th Aerospace Sciences Meeting and Exhibit*, AIAA Paper 96-0676, Reno, NV, 1996.

[35]Ballard, J. D., Orloff, K. L., and Luebs, A. B., "Effect of Tip Shape on Blade Loading Characteristics for a Two-Bladed Rotor in Hover," *Proceedings of the 35th Annual American Helicopter Society Forum*, 1979.

[36]Leishman, J. G., "On Seed Particle Dynamics in Tip Vortex Flows," *Journal of Aircraft*, Vol. 33, No. 4, 1996, pp. 823–825.

[37]Leishman, J. G., Baker, A., and Coyne, A. J., "Measurements of Rotor Tip Vortices Using Three-Component Laser Doppler Velocimetry," *Journal of the American Helicopter Society*, Vol. 41, No. 4, 1996, pp. 342–353.

[38]Devenport, W. J., Rife, M. C., Liapis, S. I., and Follin, G. J., "The Structure and Development of a Wing-Tip Vortex," *Journal of Fluid Mechanics*, Vol. 312, 1996, pp. 67–106.

[39]Leishman, J. G., "On the Aperiodicity of Helicopter Rotor Wakes," *Experiments in Fluids*, Vol. 25, 1998, pp. 352–361.

[40]Han, Y. O., Leishman, J. G., and Coyne, A. J., "On the Turbulent Structure of a Tip Vortex Generated by a Rotor," *AIAA Journal*, Vol. 35, No. 3, 1997, pp. 477–485.

[41]Coyne, A. J., Bhagwat, M. J., and Leishman, J. G., "Investigation into the Rollup and Diffusion of Rotor Tip Vortices Using Laser Doppler Velocimetry," *Proceedings of the 53rd Annual American Helicopter Society Forum*, 1997.